Conductivity Degradation of Polyvinylidene Fluoride Composite Binder during Cycling: Measurements and Simulations for Lithium-Ion Batteries

Anne M. Grillet,[a,z] Thomas Humplik,[a] Emily K. Stirrup,[a] Scott A. Roberts,[a,*] David A. Barringer,[a] Chelsea M. Snyder,[b,c,] Madison R. Janvrin,[a] and Christopher A. Apblett[c]**

[a]*Thermal/Fluid Component Sciences Department, Sandia National Laboratories, Albuquerque, New Mexico 87185, USA*
[b]*Materials and Science Engineering Department, Rensselaer Polytechnic Institute, Troy, New York 12180, USA*
[c]*Power Sources Research & Development Department, Sandia National Laboratories, Albuquerque, New Mexico 87185, USA*

The polymer-composite binder used in lithium-ion battery electrodes must both hold the electrodes together and augment their electrical conductivity while subjected to mechanical stresses caused by active material volume changes due to lithiation and delithiation. We have discovered that cyclic mechanical stresses cause significant degradation in the binder electrical conductivity. After just 160 mechanical cycles, the conductivity of polyvinylidene fluoride (PVDF):carbon black binder dropped between 45–75%. This degradation in binder conductivity has been shown to be quite general, occurring over a range of carbon black concentrations, with and without absorbed electrolyte solvent and for different polymer manufacturers. Mechanical cycling of lithium cobalt oxide ($LiCoO_2$) cathodes caused a similar degradation, reducing the effective electrical conductivity by 30–40%. Mesoscale simulations on a reconstructed experimental cathode geometry predicted the binder conductivity degradation will have a proportional impact on cathode electrical conductivity, in qualitative agreement with the experimental measurements. Finally, ohmic resistance measurements were made on complete batteries. Direct comparisons between electrochemical cycling and mechanical cycling show consistent trends in the conductivity decline. This evidence supports a new mechanism for performance decline of rechargeable lithium-ion batteries during operation – electrochemically-induced mechanical stresses that degrade binder conductivity, increasing the internal resistance of the battery with cycling.
 [DOI: 10.1149/2.0341609jes]

Manuscript submitted May 18, 2016; revised manuscript received June 20, 2016. Published July 2, 2016. This was Paper 368 from the San Diego, California, Meeting of the Society, May 29- June 2, 2016.

Lithium-ion batteries (LIB) are an enabling energy storage technology for portable consumer electronics, electric vehicles and renewable power generation in part due to their high energy densities. The energy density is driven by not only the relatively large potential of lithium-ion chemistries, but also the ability of active materials to store large amounts of lithium.[1] The most common graphitic carbon anode can absorb up to one lithium for every carbon atom. Recent research on higher capacity anodes such as silicon has highlighted an increased need for understanding the mechanics of lithium-ion batteries. As the lithium is shuttled between the anode and cathode, the active materials expand and contract to accommodate the lithium. The resulting volume changes are accentuated for high capacity materials such as silicon which can increase in volume by up to 400% during lithiation.[2]

Because most LIB electrodes are porous multicomponent composites, understanding the generation and impact of mechanical stresses on batteries can be difficult. The electrode is generally 50–75 vol% solid fraction with active material consisting of micron-sized particles held together by an active binder, which is itself a composite of conductive carbon particles and polymer. The performance of the battery is highly dependent on this complex structure which must allow efficient ion and electron transport through the electrode. The void space in the porous structure allows lithium ions in the electrolyte to access most of the surface area of the active material. The composite binder and active material provide an electronically conductive path for the electrons to travel from the current collector throughout the electrode. The dispersed active material particles provide a large surface area for the electrochemical reactions which is critical for drawing large currents from the battery. The composite polymer-carbon black binder plays key mechanical and electrochemical roles in the battery operation - physically holding the electrode together as well as providing electron conduction paths through the electrode. For simplicity, we will use the term *binder* to refer to the composite of polymer and conductive additive. The polymer traditionally used for lithium-ion batteries is polyvinylidene fluoride (PVDF) primarily because of its excellent resistance to the large electrochemical potentials found in these batteries. Despite not being ideal in other respects, PVDF has been successfully used for decades to manufacture commercial lithium-ion batteries.[3]

Next generation high capacity battery active materials have highlighted several battery failure mechanisms driven by volume changes and the resulting generation of mechanical stresses including pulverization of the active material, loss of contact with the current collector, cracking and reformation of the SEI passivation layer and loss of electrode porosity restricting ionic conduction.[2,4–7] Silicon is an extreme example of volume change, but most battery active materials undergo some volume change during cycling which can result in mechanical stresses within the battery in addition to stresses that are imposed by the manufacturing process.[7,8] The vast majority of lithium-ion batteries undergo particle swelling and hence electrode swelling during cycling, a process sometimes referred to as electrode breathing. To the extent that the breathing is irreversible, these mechanical processes may contribute to battery performance degradation after cycling or capacity fade.

Even in traditional lithium-ion batteries, cycle driven electrode breathing occurs and there is evidence it can strongly affect the performance of the battery. The most common commercial chemistry is a lithium cobalt oxide ($LiCoO_2$) cathode paired with a graphitic carbon anode. The anode is usually not the capacity limiting electrode. Upon charge, the graphite anode increases in volume up to 12.8% as the lithium ions infiltrate between the graphitic planes of the carbon.[8] The volume response in the cathode

*Electrochemical Society Member.
**Electrochemical Society Student Member.
[z]E-mail: amgrill@sandia.gov

is more complex. Normally, this battery chemistry is charged to a cathode lithium concentration of $Li_{0.5}CoO_2$ where only half of the existing lithium capacity is utilized. As lithium is extracted from the layered crystal structure, the adjacent negatively charged oxygen layers are no longer screened causing the crystal to expand by ∼1.5% along the c-axis during delithiation to a concentration of $Li_{0.5}CoO_2$.[9,10] Interestingly, if additional lithium is removed, there is a large reversal in the volume change with the oxide crystal shrinking by almost 10% upon full delithiation to CoO_2.[10] Fully delithiating the $LiCoO_2$ is only partially reversible, perhaps in part due to the larger volume changes and resulting mechanical stresses.

With relatively modest volume changes for the $LiCoO_2$ - graphite battery chemistry, one might expect that the mechanical changes are negligible, but there is evidence to the contrary. In a study of prismatic cells, Rubino et al.[11] found that graphite anodes irreversibly swelled after cycling, resulting in an increase in porosity. Capacity fade in these cells could be recovered by recalendering the anodes to the originally density. The capacity fade was more apparent in prismatic cells than in cylindrical cells where the rolled geometry would provide a confining pressure on the electrodes. Qi and Harris[12] created a custom battery to directly observe the lithiation of a graphite electrode in situ. They found expansion of graphite translated into macroscopic strains of the electrode using digital image correlation. Recent experiments by Cannarella and Arnold[13] highlight the role of electrode breathing by confining a prismatic cell between fixed platens and monitoring the stresses generated during cycling. Not only does the battery expand on charging, resulting in an increase in measured stress, but that process is only partially reversible as evidenced by an increase in confining pressure during extended cycling. Confining pressure was hypothesized to reduce battery capacity by limiting ion mobility resulting in loss of active lithium through lithium plating on the anode surface.[13,14]

Another mechanism proposed to explain capacity fade is through particle isolation. As active material particles get separated from the electrically conductive pathways in the electrode, they no longer contribute to the cycling capacity of the battery. Isolation of active material particles can occur due to the electrode breathing as described above[7] or if the active material particles fracture under the mechanical stresses induced during charging.[5,15]

The most common polymer for battery applications is polyvinylidene fluoride, a fairly stiff semi-crystalline polymer with a Young's modulus in the range of 1.5–2.5 GPa.[16–19] The glass transition temperature of PVDF is −30°C and the melting temperature is 154–184°C.[20] In battery applications, the polymer will absorb the organic carbonate solvent of the electrolyte[21] which reduces the modulus while allowing it to remain a rubbery solid; presumably due to the long lived crystalline crosslinks between polymer chains. Even in the swollen state, PDVF is not very extensible, failing at a strain of only 4%.[22] By itself, PVDF is neither ionically nor electronically conductive.[21,23] In fact, it has also been proposed as a material for lithium-ion battery separators.[21] To add electronic conductivity, PVDF is mixed with a conductive acetylene black or carbon black (CB) additive. If the concentration of conductive carbon is greater than the percolation threshold of ∼15 wt%,[24] then the conductivity of the composite increases up to ∼1 S/cm.[25] The carbon black may be aggregated within the binder which may contribute to the low percolation threshold and high conductivity.[26] The fraction of conductive carbon in the binder is generally higher in the cathode where the electronic conductivity of the active material is lower than the anode. Within the composite electrodes, the binder makes up a small fraction of both the cathode and anode (∼6 wt% in our research-grade electrodes) and is believed to be located primarily in the small spaces between particle contacts.[24,27] This binder morphology might be driven by capillary stresses as the solvent used to manufacture the electrodes evaporates. This position is advantageous for both electrical and mechanical roles of the binder. In particular, since the polymer is much softer than the active materials (graphite - E=32 GPa, $LiCoO_2$ - E=149 GPa),[15,28] the presence of binder between particle contacts softens the composite electrode compared to the active material. Tensile measurement of a 70 wt% $LiCoO_2$ composite with binder had a combined Young's modulus of 2.7 GPa, far below that of pure $LiCoO_2$.[26]

Much of the continuum-level modeling of battery operation has assumed the properties for the binder can be absorbed into an average representation of other phases,[6] but particle-scale modeling has provided insight into how the binder affects mechanical stress development. Awarke et al.[18] represented the electrode as a three-dimensional box of spheres and then took a very simple approach of filling all of the void space with binder. As the particles swelled, they found that the mechanical stress in the binder was primarily localized between the particle contacts. Rahani and Shenoy[17] modeled several representative binder distributions in two dimensions: binder located just between particle contacts and binder uniformly coating the spherical particles. The average in plane stresses over a range of material properties agreed to within 10% for the two binder morphologies. Their simulations also showed that the mechanical stresses were localized between particle contacts, even when the binder was assumed to uniformly coat the particles. The average stresses were also found to depend strongly on the thickness of the binder (which also controlled the separation between the active material particles).

While those studies assumed that the particles were spherical, real active material particles have much more complex shapes. Recent modeling studies by Mendoza et al.[29] have used experimentally derived three dimensional $LiCoO_2$ cathode microstructures to look at the development of mechanical stresses as the particles swell during charging. Their simulations assumed that the binder uniformly coated the particles and predicted the effective modulus of the composite cathode as a function of the amount of binder. Bumpy and rough particle shapes result in more heterogeneous particle contacts, but the trend was consistent with the previous work. Binder was found to play an important role in mitigating the mechanical stresses which are generated during cycling, decreasing the maximum calculated stress by 50% for a 100 nm thick layer of binder. If we consider the other important role of the polymer binder - improving electronic conductivity - the binder coating on the active material particles should be equally important in providing conduction pathways through the electrodes, especially in the cathode due to the low electronic conductivity of $LiCoO_2$.[30]

The binder plays two important roles in lithium-ion battery performance, but its contribution to cycling degradation has not been previously explored. In this work we examine the mechanical and electrical properties of binder consisting of polyvinylidene fluoride polymer with conductive carbon additive and how those properties evolve during cycling. First, the experimental methods are described, followed by a discussion of the mechanical properties of the binder. The evolution of the binder electrical conductivity as a result of mechanical cycling is probed in detail. Then experimental results on $LiCoO_2$ cathodes subjected to mechanical cycling and mesoscale numerical simulations on the mechanisms for conductivity degradation will be discussed. Comparisons will be made between the binder electrical conductivity evolution and measurements of ohmic resistance in electrochemically-cycled coin-cell batteries. Finally, the Conclusions section will integrate the presented data and propose a new mechanism for performance decline in lithium-ion batteries due to degradation of the composite binder caused by cyclic mechanical stresses generated during electrochemical cycling.

Experimental

Lithium-ion batteries typically use polyvinylidene fluoride mixed with conductive carbon particles as the electrode binder. The majority of this study used battery grade Solvay 5130 PVDF and Denka acetylene black conductive additive. To make composite binder films for testing, the PVDF is dissolved in warm 1-methyl-2-pyrrolidione using an IKA RW20 stand mixer at 500 rpm and 50–70°C under a nitrogen gas blanket for two hours. The carbon is added and mixed at 1800 rpm for 2 hours to ensure good dispersion of the particles. The slurry is degassed at room temperature under vacuum for one hour and then cast onto a flat inert substrate. Finally, the film is dried in a vacuum oven at 90–110°C for 12 hours resulting in a film thickness of 70–250 mi-

crons. The composite binder film is carefully peeled off the substrate once dry and cut into bars for mechanical testing or punched into disks for cycling studies. The effect of solvent interactions are studied after soaking the films for at least 12 hours to ensure equilibrated solvent absorption. Solvents used included propylene carbonate (PC) from Sigma-Aldrich, ethylene carbonate (EC) from Mitsubishi Chemical Company, and ethyl-methyl carbonate (EMC) from Kishida Chemical Company.

$LiCoO_2$ electrodes consisted of nominally 94 wt% $LiCoO_2$ (LICO Technology), 3 wt% polyvinylidene fluoride (PVDF) (Kureha W #1300), and 3 wt% carbon black (Denka) mixed in 1-methyl-2-pyrrolidione to make a viscous slurry. The cathode slurry was cast onto carbonized aluminum foil using a laboratory scale doctor blade coater (Elcometer, Byk blades) and had a dry coating thickness of ~50 μm. The coating was air-dried overnight and then dried under vacuum at 110°C for 12 hours. For full cell testing, a similar procedure was used to fabricate graphite electrodes with 92 wt% Graphite (ConocoPhillips G8), 6 wt% PVDF (Kureha 9200), and 2 wt% carbon black (Denka). The anode slurry was cast onto copper foil and had a dry coating thickness of ~70 μm.

Since many lithium-ion battery electrolyte solvents are volatile, working with solvent mixtures can lead to uncertainty in the mixture composition as a function of time. For example, if ethyl methyl carbonate is evaporating from a mixture with ethylene carbonate, the fraction of ethylene carbonate increases with time. To avoid the potential uncertainty in composition, we have primarily used pure propylene carbonate to measure the properties of solvent swollen battery components. Propylene carbonate has a relatively low evaporation rate and with a single component the composition was consistent throughout the experiment. Babinec et al.[26] found only small differences between the measured Young's modulus and strain to failure of binder films saturated with pure propylene carbonate and a mixture of ethylene carbonate with diethyl carbonate. Our own measurements comparing propylene carbonate to other solvent mixtures also found only small differences in the measured Young's modulus and solvent uptake as will be reported in the next section. Using pure solvent also simplifies the electrical impedance spectroscopy measurements for without lithium salts in the electrolyte, the composite binder and cathode films are purely resistive.

Mechanical measurements of the binder films are performed in a Netzsch Artemis Dynamic Mechanical Analyzer in tensile testing mode. The Young's modulus of the dry binder films was measured as a function of temperature from 25–65°C and frequencies of 1 and 10Hz. Swollen samples were measured using a solvent immersion cell to keep the binder samples surrounded by solvent during the measurement.

The impact of mechanical cycling was studied using an Anton Paar Modular Compact Rheometer (MCR502) in a parallel plate geometry which allowed controlled cyclic compression of the binder with up to 50 N force (2.5 MPa pressure) at controlled ramping rates. The measurement fixtures were modified from a dielectric measurement tool-kit sold by Anton Paar which provides 25 mm diameter parallel plates which are electrically isolated from the rest of the rheometer by ceramic spacers. Low resistance electrical connections were created by welding wire leads to the backs of the parallel plates. These leads were connected to a Metrohm PGASTAT204 with an FRA 32 electrical impedance spectroscopy module. To provide a clean surface for measurements, 16 mm (5/8″) diameter disks of copper current collector were attached to the plate surfaces with Kapton tape.

Because the binder films are thin and fairly stiff, cycling studies were carried out on stacks of disks in order to achieve more accurate strain measurements. Groups of six 4.8 mm (3/16″) disks were punched from the same binder film and stacked into a cylinder. Sample height measurements were corrected for machine compliance by performing force cycling on a sapphire disk. Sapphire has a modulus of >200 GPa and was assumed not to deform during the experiment. The measured deviations in the gap were fit with a third order polynomial which captured the machine compliance to within ±2 μm over the range of 10–50 N. The gap film thicknesses were corrected as a function of force for all the results shown here. Typical sample heights were greater than several hundred microns and measured strains ranged from 20–50 microns; thus the error in the strain measurements was between 4–10%. Since the reported conductivities are linear in the measured sample height this contributes a similar absolute uncertainty to the conductivity measurement. Machine compliance at 50N was reproducible over multiple cycles to within a standard deviation of 0.2% so comparisons at the same applied force will have much lower uncertainty.

Performance of the electrical impedance system was verified with a number of tests. Contact resistance between the bare plates was measured to be lower than 0.1 ohm. The lowest sample resistances measured were in the range of 2 ohms, well above this contact resistance. Additionally, measurements of a set of resistors from 2–1000 ohms were measured to within a few percent and confirmed to be independent of frequency. The dielectric constant of PVDF sheets (Solvay 9009) were measured to be 7.1, within 6% of the manufacturer's specification of 7.5. Finally an ideal Randall's circuit from the Metrohm calibration box was connected to the instrument and the series and the individual component resistances were determined within a few percent. These verification tests give us confidence that this combined tool can accurately measure a variety of mechanical and electrochemical responses.

Mechanical Properties of Polyvinylidene Fluoride-Carbon Black Binder Films

Mechanical characterization was performed on composite binder films to determine their average properties and understand the influence of carbon black fraction and absorbed solvent. Studies were performed on a series of binder films with carbon black concentrations ranging from 0–40 wt%. Cross sections of representative binder films are shown in Figure 1. All of the binder films exhibited significant porosity (45± 10%). At a carbon black concentration of 20 wt% (Figure 1a), there were regions of pure polymer in the film, while at a higher carbon black concentration of 40 wt% (Figure 1b), all of the polymer was drawn into the interstitial spaces between the particle aggregates.

The PVDF - carbon black binder films exhibited primarily elastic behavior with some viscoelastic or time-dependent response. Figure 2 shows the elastic (storage) and viscous (loss) moduli for a 20 wt%

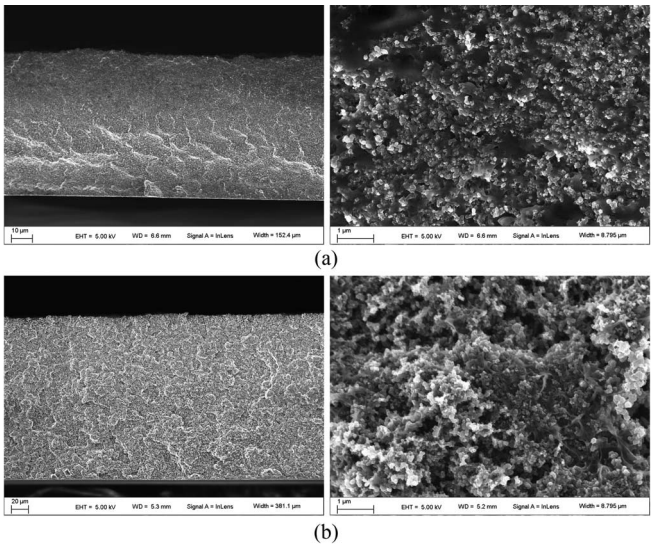

Figure 1. Scanning electron micrographs of dry uncycled polyvinylidene carbon black films for 20 wt% (a) and 40 wt% (b) carbon black fractions. For the lower carbon fraction, the polymer is able to completely coat the carbon and create a cohesive matrix. At the higher carbon black weight fraction, the polymer cannot fill the space between the carbon black aggregates.

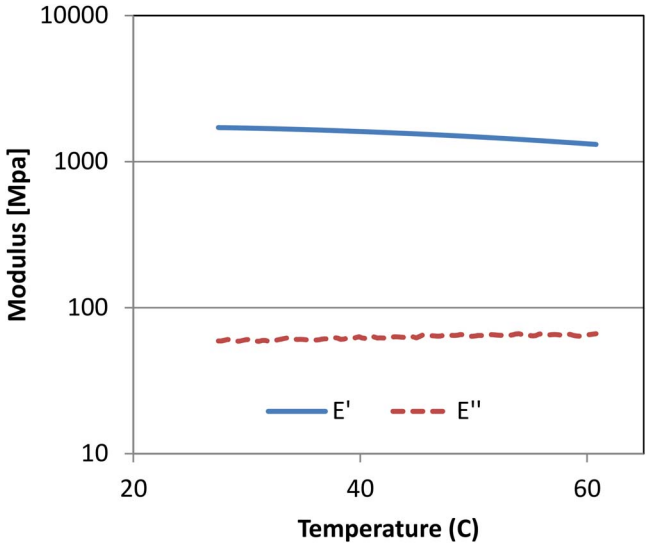

Figure 2. Elastic E′ and viscous E″ moduli as a function of temperature for a dry uncycled 20 wt% carbon black binder film showing that the elastic response dominates. The moduli are only weakly temperature dependent.

carbon black film as a function of temperature at a frequency of 1 Hz and an applied strain of 0.1%. The elastic modulus is roughly 2 GPa at room temperature, in good agreement with published literature.[16,18] The modulus decreases gradually by 25% as the temperature is increased to 65°C. The viscous modulus is lower than the storage modulus by over an order of magnitude and increases slightly with temperature. As a first approximation, the binder responds as an elastic solid, but a viscoelastic response was apparent on longer time scales in the mechanical cycling testing.

Despite the large differences in morphology, the mechanical properties of the composite binder films are not strongly dependent on the carbon black volume fraction. Figure 3a shows that the measured elastic moduli for carbon black concentrations from 0–40 wt% averaged 2.4 ± 0.4 GPa as summarized in Table I. Each point was averaged over 3-5 measurements and the error bars show the 95% confidence interval of the mean. The modulus of the carbon black composites is larger than the pure polymer, but decreases by ∼20% as the carbon black fraction increases to 40 wt%.

Binder films absorb a significant amount of carbonate solvent as seen in Figure 3b. Interestingly, solvent absorption increases with higher carbon black fractions in the binder film. Though the carbon black isn't expected to swell the way the polymer does, it may contribute by drawing solvent into the pores of the particle aggregates. There was not a significant difference in measured solvent uptake for the composite binder between pure propylene carbonate and a 1:1 mixture of ethylene carbonate and propylene carbonate. Likewise, the choice of PVDF supplier had only a modest impact on solvent absorption for the 20 wt% carbon black binder films. All of the composite binder samples reached steady-state solvent absorption within four hours. Figure 3a shows an average elastic modulus for swollen binder films of ∼200 MPa in agreement with the literature.[26] The swollen binder exhibited a similar dependence on carbon black weight fraction as the dry films. The elastic moduli for binder films swollen in a 3:7 mixture of ethylene carbonate:ethyl methyl carbonate are also shown for comparison. The measured moduli are slightly lower, but consistent with the propylene carbonate measurements so the conclusions drawn from experiments in propylene carbonate should also apply to other solvent compositions.

Table I. Elastic modulus for polyvinylidene fluoride - carbon black binder as a function of carbon black concentration showing both DMA elastic modulus in tension and effective compressive modulus from mechanical cycling experiments.

CB wt%	DMA dry [MPa]	DMA swollen [MPa]	Compression Dry [MPa] 2nd cycle–166 cycle	Compression Swollen [MPa] 2nd cycle–166 cycle
10 wt%	2600.4	238.5	49.6–59.4	38.5–42.9
20 wt%	2831.0	246.8	56.4–70.4	50.4–56.1
30 wt%	2142.3	183.9	52.1–63.9	32.6–37.6
40 wt%	1994.4	125.3	107.1–128.8	70.0–75.8

Mechanical Cycling of Polyvinylidene Fluoride-Carbon Black Binder Films

Electrical conductivity measurements were performed on dry and electrolyte solvent swollen binder films as a function of force and with repeated mechanical cycling. Based on the results of Mendoza et al.,[29] the mechanical stress within an electrode increases linearly with the state of charge. Thus to mimic the effects of mechanical stresses inside of a cycling battery, we subject the binder films to stress cycles where the applied force is linearly increased.

Dry composite binder films.—Figure 4 shows the results of the first 2 mechanical cycles on a 30 wt% carbon black binder. The force applied to the binder was ramped from a minimum of 27 kPa (enough to maintain contact with the electrodes) up to 2800 kPa with an effective rate of 4C (meaning that the force was ramped to reach the maximum stress in 1/4 hour). The maximum stress ap-

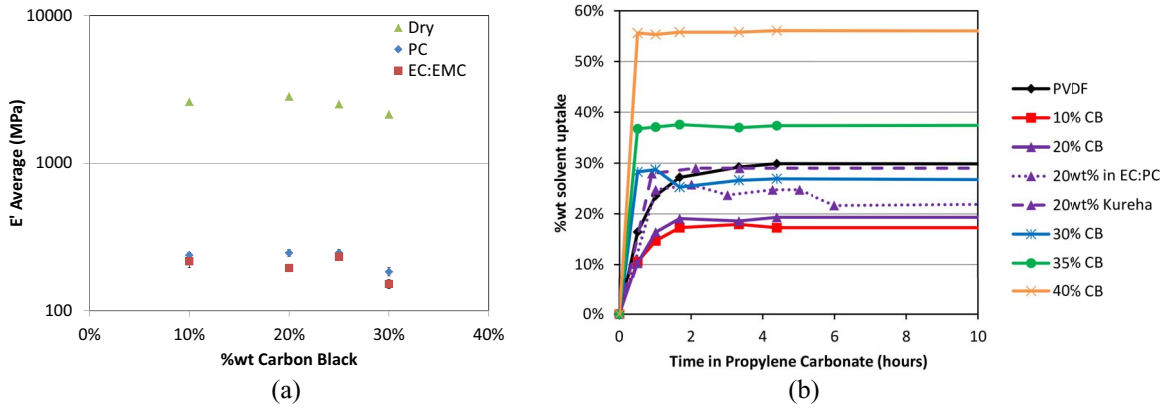

Figure 3. Mechanical properties of uncycled polyvinylidene fluoride - carbon black binder: (a) The elastic modulus as a function of carbon black weight fraction. Measurements are taken at 1 Hz frequency and a strain of 0.1% for dry binder and 1.5% for solvent swollen binder. The error bars represent the 95% confidence interval of the mean for several measurements. (b) Solvent absorption as a function of time for various carbon black weight fractions.

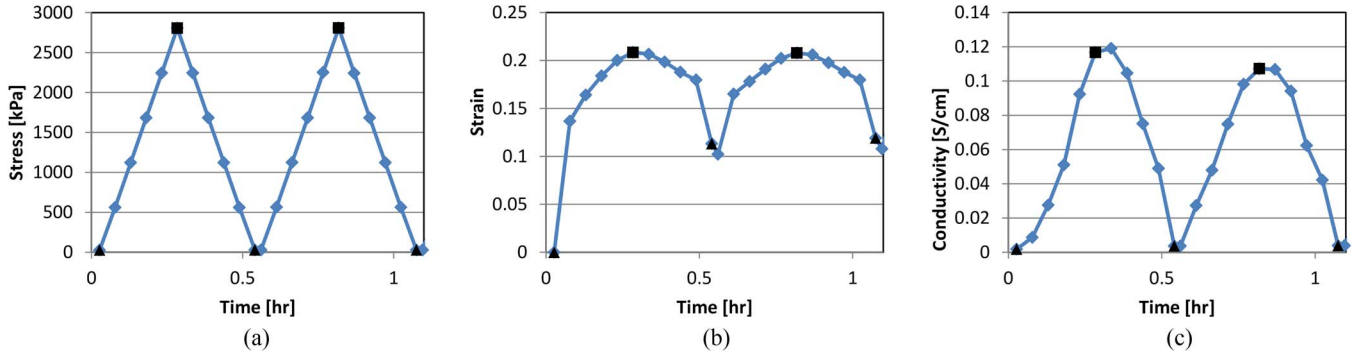

Figure 4. First two mechanical cycles of dry 30 wt% carbon black binder film showing the applied stress and resulting strain and electrical conductivity. The peak and minimum values of the strain and conductivity are marked by squares and triangles respectively. (a) Stress [kPa]; (b) Strain. (c) Conductivity [S/cm].

plied was in the range of the high stresses applied by Cannarella and Arnold[13] though still below the predicted maximum stresses predicted by Mendoza et al.[29] As we will show, the cycling strains on binder films in our experiments are ∼5–10% which is in the range of the changes in electrode thickness measured by others.[7,12,28] Mendoza et al.[29] demonstrated that electrode strains are amplified in the binder because the binder is much softer than the active material. The maximum stress of 2800 kPa was determined to be a reasonable balance between applying realistic strains, maintaining the sample sizes in a workable range and staying within the limitations of the instrument.

The strains shown in Figure 4b are calculated relative to the sample height at the initial loading stress of 27 kPa. During the first cycle, the binder shows a strain of approximately 21%. The majority, but not all, of that deformation was reversible. The irrecoverable deformation after the first cycle was much larger than measured for subsequent cycles and may be due to flattening of the multiple disks and/or removal of porosity from the film. Although the binder exhibits a primarily elastic response, there is also evidence of viscoelasticity in the cycling data. When the force is held at 28 kPa for two minutes in between mechanical cycles, the stress continued to recover as seen in Figure 4b. The strain in the second minute was always a little bit less than the first measurement.

At each point marked on the stress curve, the force ramp was paused for a minute and electrical impedance spectroscopy (EIS) was performed over a range of frequencies from 1 Hz to 500 kHz at an amplitude of 0.1 mA. For these films, the material response was purely resistive so the measured resistance was averaged and scaled with the sample height and area to determine the conductivity of the binder. As shown in Figure 4c, the conductivity of the binder increases as the applied force increases. The compression of the film would push the carbon black aggregates together and reduce the internal resistance and also may collapse internal voids. When the force was removed, the conductivity recovered to almost its initial value. There was a slight, but reproducible phase lag in the conductivity. The maximum conductivity in a cycle was frequently at the first point of the relaxation, not at the peak force. The mechanism for the lag is not clear.

The degradation of the binder was progressive. Figure 5 plots the strain and conductivity at the maximum (2800 kpa) and minimum (28kPa) applied stresses throughout ten cycles for the dry 30 wt% carbon black binder. The strains are calculated relative to the sample height at the minimum stress after the first compression due to the observed irreversible strain during the first compression. We also define a *cycling strain* as the change in strain between the peak and minimum stress values for a given cycle. Over ten cycles, the peak strain was quite consistent, but the recovery after each compression was incomplete and the binder slowly compacted over cycling. The changes in the mechanical strain response were quite small compared to the observed changes in the conductivity shown in Figure 5b. After just 10 cycles, the conductivity of the binder at the peak applied stress decreased to 54% of its initial value.

The measured binder conductivity continued to degrade over hundreds of cycles. To keep the test length manageable, many fast cycles were interspersed between slower cycles at 4C. As shown in Figure 6, after each 4C cycle, the sample was cycled rapidly 10 times at an effective rate of 120C in order to accelerate degradation. The state of the sample was again probed over another 4C cycle with integrated pauses for conductivity measurements. Note that the changes in the mechanical response continued to be quite modest. The peak strains remained constant at ∼9% while the minimum strain continued to creep up showing that the binder continues to diminish in height, losing 3.3% of the film height after the first cycle. The diameter of the

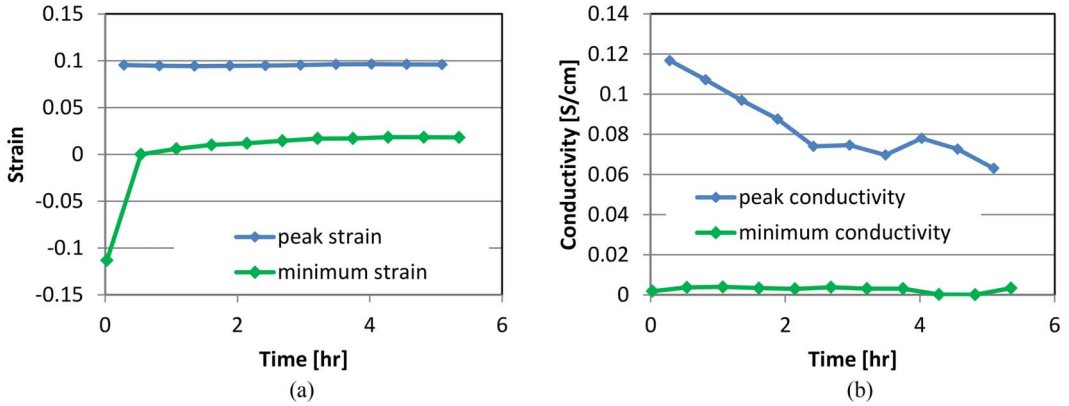

Figure 5. Results for 10 cycles at a 4C rate for dry 30 wt% carbon black binder film showing the progressive decline in the measured strain (a) and electrical conductivity (b). The peak and minimum values of the strain and conductivity are marked by squares and triangles respectively.

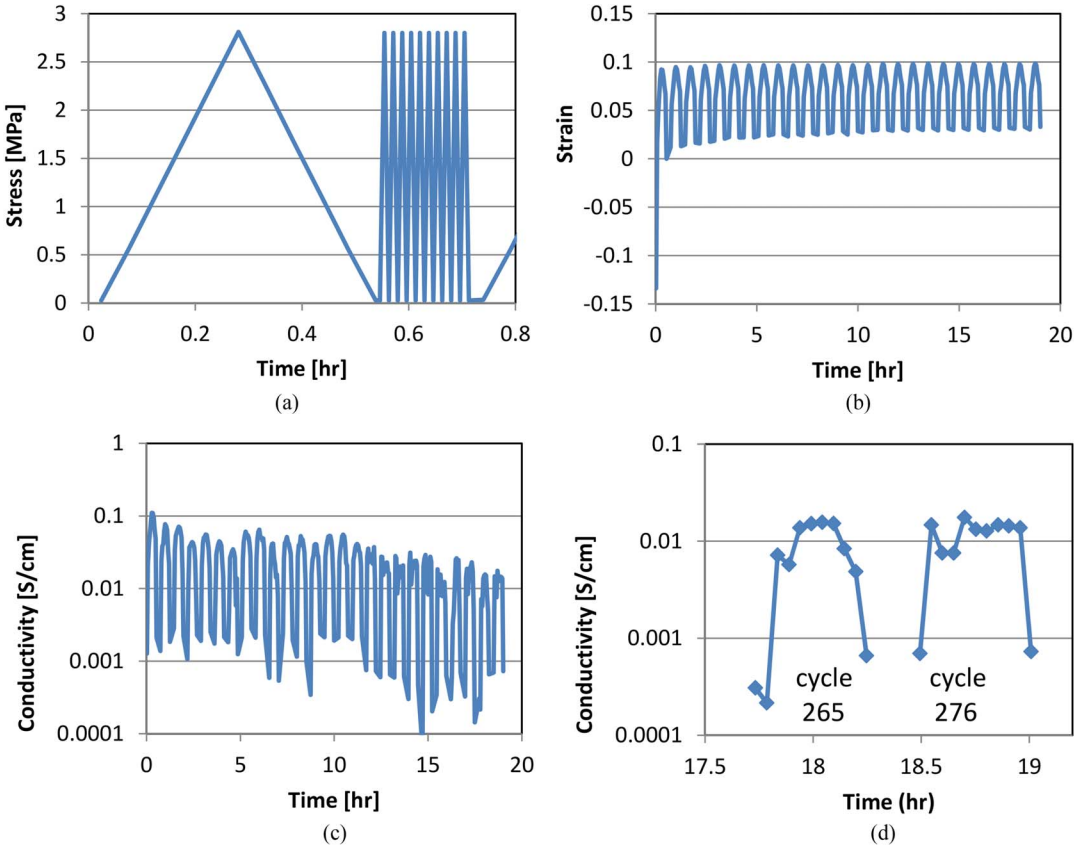

Figure 6. Results for 276 cycles of dry 30 wt% carbon black binder film showing the applied stress and measured strain and conductivity. (a) Cycling pattern with one cycle at a 4C rate where the conductivity is measured as a function of applied stress followed by 10 cycles at an 120C rate; (b) Strain as a function of time for 266 cycles. (c) Conductivity as a function of time for 266 cycles. Each displayed cycle is interspersed with 10 cycles at 120C where conductivity is not measured. (d) Conductivity as a function of time for cycle 265 and 276 showing that conductivity is no longer a monotonic function of stress.

disks was not found to increase after mechanical cycling suggesting that the measured height change was due to a densification of the composite binder film which could restrict ionic transport.

Despite the modest mechanical changes, there continued to be substantial changes in the conductivity. The rate of conductivity decline was slower than was observed with repeated 4C cycles. After 11 cycles, the accelerated cycling test exhibited a 30% decline in the conductivity compared to a decline of 54% when all of the cycles were slow. Because of the viscoelasticity of the binder, we expect some rate dependence and the faster cycles may not have experienced as large of a strain as the slower cycles. Nonetheless, the conductivity continued to decline significantly with additional mechanical cycles as shown on a log scale in Figure 6c to accentuate the changes at the minimum applied force. The mechanical cycling degraded the peak conductivity of the binder by 82% from the initial value of 0.110 S/cm to 0.048 S/cm after 266 cycles. The conductivity at the minimum applied stress also declined by almost 80% in this test from a value of 2.68×10^{-3} S/cm after the first cycle to 0.56×10^{-3} S/cm. The conductivity decline was surprising given that over many cycles, the film is becoming more compact and denser which one would expect to increase the conductivity. The force dependence of the conductivity also changes after cycling. While the mechanical strains have a similar dependence on the applied stress as shown in Figure 4b, the measured conductivity no longer increased monotonically with the applied stress. Instead the conductivity seemed to plateau as the applied stress increased as shown in Figure 6d.

We also investigated the dry polyvinylidene fluoride-carbon black binder films as a function of carbon black concentration in Figure 7. As expected, increasing the carbon black concentration increased the conductivity of the binder. For each carbon black concentration measured, a significant decrease was observed in the conductivity after the first 11 cycles. Figure 8 shows the progressive degradation of the peak conductivity of dry binder as a function of carbon black concentration over 166 cycles. For carbon black concentrations from 10 wt% through 40 wt%, the peak conductivities showed a consistent trend of substantial decrease after cycling between 55–75% for all carbon black concentrations as summarized later in Table II.

Scanning electron images of cycled binder films are shown in Figure 9. No cracks or other disruptions of the film morphology were observed relative to the uncycled films shown in Figure 1. The polymer was still adhered to the carbon black and the carbon black aggregates appear whole. Despite the densification, the films still appeared porous. From these images, the physical mechanism for the conductivity degradation is not clear.

Electrolyte solvent swollen composite binder films.—Mechanical cycling degradation was also examined for binder saturated with propylene carbonate solvent. The binder disks were found to absorb solvent and swell from an initial diameter of 4.8 ± 0.1 mm to 5.03 ± 0.1 mm with no noticeable dependence on carbon black composition. Strain and conductivity measurements are shown in Figures 10 and 11 for carbon black fractions from 10 wt% up to 40 wt%. No increase in disk diameters was noted after cycling.

Several differences are noted between the swollen and dry binder response. First, the dry conductivity data tended to have greater variability, perhaps because the stiffer dry binder can't accommodate as easily to the rigid plates. Also, the compressive strains tended on average to be larger for the solvent swollen samples. Although the dry binder has a larger modulus than the swollen binder, the magnitude of the strain difference is much smaller than expected. The slope of the

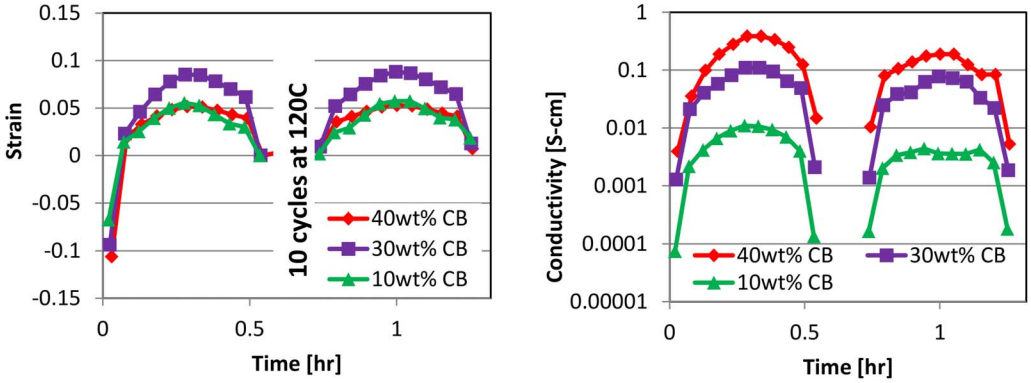

Figure 7. Strain (a) and electrical conductivity (b) during the first 12 cycles of mechanical cycling for dry polyvinylidene fluoride-carbon black binder for several carbon black concentrations.

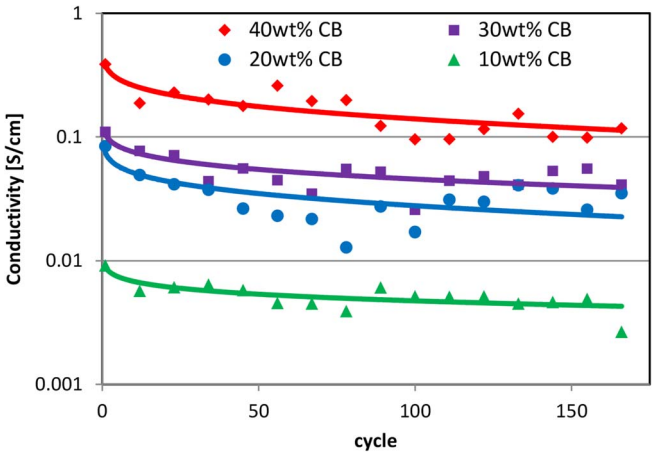

Figure 8. Progressive degradation of electrical conductivity at the peak applied stress for dry polyvinylidene fluoride-carbon black binder as a function cycle for several carbon black concentrations. Data points are averaged over several experiments at each carbon black fraction.

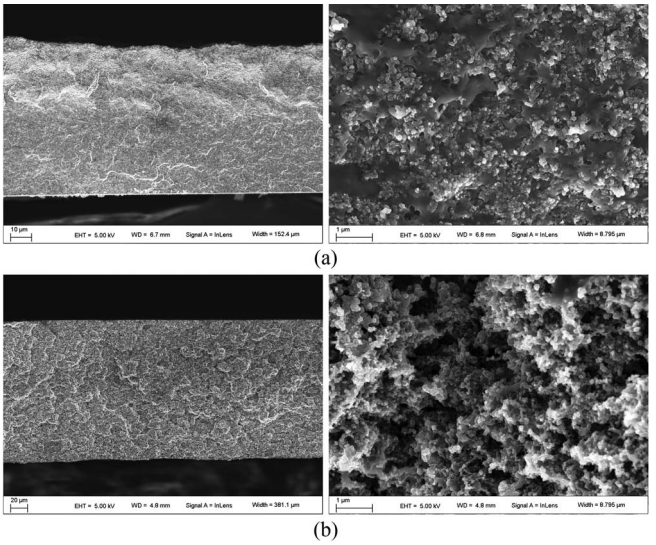

Figure 9. Scanning electron micrographs of cycled dry polyvinylidene fluoride - carbon black films for 20 wt% (a) and 40 wt% (b) carbon black fractions. For the lower carbon fraction, the film was mechanically cycled 266 times and the 40 wt% film was cycled 166 times. No obvious changes in morphology are observed relative to the uncycled binder films shown in Figure 1.

stress-strain curve was very linear between 10 and 40 Newtons of applied force allowing an effective compressive modulus to be calculated from these experiments. The compressive modulus was compared to the elastic moduli measured with the dynamic mechanical analyzer in Table I. The compressive moduli were noticeably smaller than the elastic moduli measured in tensile testing. Though the swollen films experienced larger strains, a larger fraction of that strain was recovered once the stress was released leading to less consolidation of the binder film with cycling as shown in Figure 11. The dry films lost an average of 2.6% of their height between the 2nd and 166th cycle, while the swollen films only lost 1.9% of their height on average.

Effect of polyvinylidene fluoride manufacturer.—To ensure the observed degradation was not specific to Solvay 5130 battery grade polyvinylidene fluoride, commercially available battery grade PVDF - Kureha W #1300 was also tested. Composite binder films containing 20 wt% carbon black were cycled under identical conditions to the Solvay material in both the dry state and also saturated with propylene carbonate. Figure 12 shows the comparison of both the cycling strain and peak conductivity for the two polymers. The binder containing the Kureha PVDF polymer exhibited slightly lower strains, but the decline in the composite binder conductivity was comparable to the binder made with Solvay polymer as shown in Table II. These results on two manufacturers suggests that

Table II. Measured decrease in the electrical conductivity for mechanically cycled polyvinylidene fluoride - carbon black binder films after 166 cycles.

PVDF	CB wt%	Dry	Swollen
Solvay	10 wt%	−56%	−45.5%
Solvay	20 wt%	−59%	−73.9%
Solvay	30 wt%	−57%	−79.0%
Solvay	40 wt%	−73%	−57.0%
Kureha	20 wt%	−66.3%	−58.4%

Table III. Percentage decrease in electrical conductivity for mechanically cycled lithium cobalt oxide cathodes and electrochemically cycled full battery cells.

Sample	Applied cycing	Conductivity change
Cathode - dry	166 mechanical cycles	−28.9%
Cathode - swollen	166 mechanical cycles	−42.4%
Cathode - simulation	166 mechanical cycles	−56%
Full cell	55 electrochemical cycles	−6.3% to −23.6%

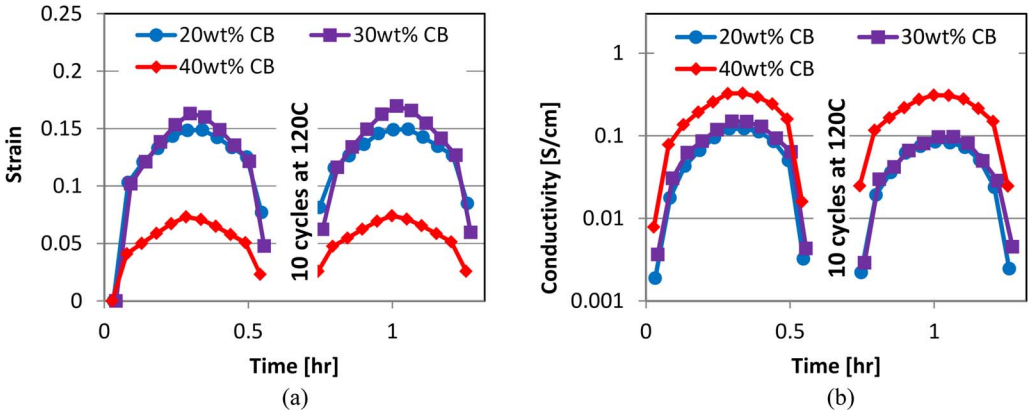

Figure 10. Strain (a) and electrical conductivity (b) during the first 12 cycles of mechanical cycling for solvent swollen polyvinylidene fluoride-carbon black binder for several carbon black concentrations.

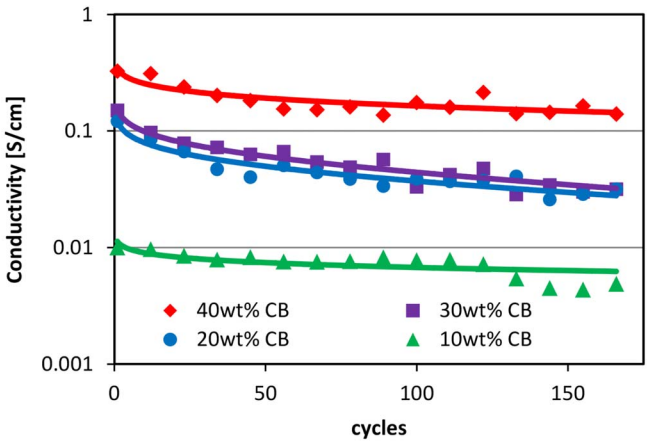

Figure 11. Progressive degradation of electrical conductivity at the peak applied stress for solvent swollen polyvinylidene fluoride-carbon black binder as a function of applied cycle for several carbon black concentrations. Data points are averaged over several experiments at each carbon black fraction.

degradation after exposure to mechanical stresses is a general property of PVDF-based lithium ion battery binders.

Mechanical Cycling of Lithium Cobalt Oxide Cathodes

Experimental measurements of lithium cobalt oxide cathodes.— If the conductivity in the binder is important in reducing the electrical resistance in the cathode, then the cathode should exhibit similar conductivity degradation to that observed in the binder films. To test this hypothesis, the conductivity of research-grade cathodes (94 wt% $LiCoO_2$: 3 wt% Kureha PVDF: 3 wt% carbon black) was measured as a function of mechanical cycling. The 4.8 mm disks were stacked with the aluminum current collector down so that the layers of aluminum and electrode alternated. The aluminum was assumed not to deform and the height of the aluminum was subtracted from the total measured height for the conductivity calculation. Figure 13 shows the measured strain and conductivity as a function of cycle number. As predicted, similar trends were observed where the measured electrical conductivity decreased with mechanical cycling.

Two noted differences in the cathode results are that the conductivities and the strains are both much lower than the composite binder. The $LiCoO_2$ active material has both a higher modulus and a lower electrical conductivity than the binder and makes up a majority (94 wt% or 86 vol%) of the cathode. Over many cycles there was still a slow loss of cathode height or densification of the cathode which could limit ion conductivity through the cathode. The electronic conductivity of the cathode also degraded; the peak conductivity decreased by 53% after 166 cycles, as summarized in Table III. Since there was no electrochemistry in these systems, the conductivity of the active material is expected to be constant. Therefore, changes in the measured conductivity must be attributed to either changes in the binder conductivity or rearrangements in the internal structure of the cathodes. Over the same number of mechanical cycles, the conductivity of the cathode decreased by 46% compared to a decrease of 55% for the solvent swollen binder with 40 wt% carbon black (the closest concentration to the cathode composition of 50 wt% carbon black in the binder). Our hypothesis is that binder degradation is the cause of the observed decrease in cathode conductivity, not structural rearrangements.

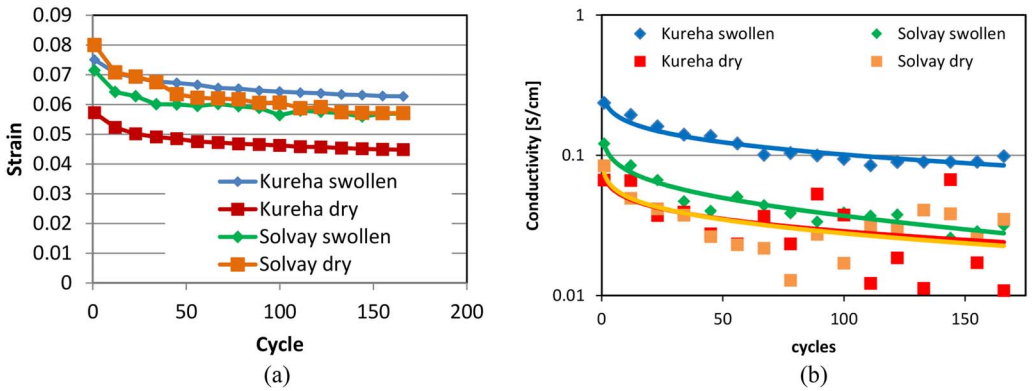

Figure 12. Comparison of cycling strain (a) and electrical conductivity (b) for 20 wt% polyvinylidene fluoride-carbon black binder made with Solvay 5130 and Kureha W #1300 polyvinylidene fluorides as a function of mechanical cycling.

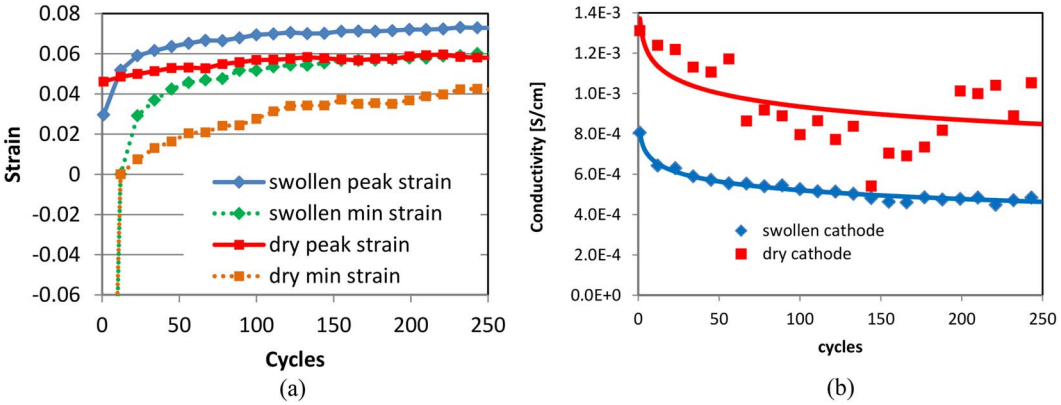

Figure 13. Strain (a) and electrical conductivity (b) at the peak applied stress of a lithium cobalt oxide cathode as a function of mechanical cycles. Data points are averaged over several experimental measurements.

Numerical simulations of lithium cobalt oxide cathodes.—Simulation results for the effective conductivity of an $LiCoO_2$ cathode with PVDF - carbon black binder were used to investigate whether the measured degradation in the binder conductivity could have caused the decline in cathode conductivity after mechanical cycling.

Simulations were performed on a reconstructed microstructure derived from energy dispersive X-ray spectroscopy (EDS) within a scanning electron microscope (SEM). A gallium focused ion beam (FIB) was used to make cross sections into the cathode. These images had a resolution (voxel size) of 256 nm × 200 nm × 250 nm. The images were reconstructed using Avizo 9 (FEI; Hillsboro, OR), surface meshed, and exported in the STL format. The Conformal Decomposition Finite Element Method (CDFEM) was used to combine a regular tetrahedral background mesh with the surface mesh into a mesh that conforms to the particle geometry. The computational domain reconstructed a piece of the cathode which was 6 μm × 6 μm × 14.3 μm with a computational background mesh size of 0.3 μm capturing 30–40 $LiCoO_2$ particles. The mathematical model was applied to our reconstructed domain and solved using Sierra Multi-Mechanics Module Aria.[31] This process of reconstruction, surface meshing, and CDFEM are described in detail by Roberts et al.[32] and was recently used by Mendoza et al.[29]

Binder was represented in this reconstructed geometry by retracting the $LiCoO_2$ particle surface slightly and replacing that retracted region with a separate binder phase as shown in Figure 14a. This method created a uniform coating of binder on the outside of all particles - a morphology proposed and used by several other researchers.[17,19,25] This approach was consistent with the mechanics calculations described by Mendoza et al.[29] Multiple binder thicknesses were explored, from 10–100 nm. Mendoza et al.[29] examined the impact of binder on the effective modulus of a cathode. They showed that the mechanical stresses tended to be localized at particle contacts so the presence of binder between particles causes a significant reduction of the cathode modulus. A volume fraction of 14% binder decreased the effective modulus by over a factor of three. We focused on simulations having a 32 nm binder thickness, which is equivalent to a dry binder composition of approximately 6 wt% or 14 vol%,[3] matching the 6 wt% experimental composition.

Electron transport is governed by the steady-state continuity equation for current density, $\nabla \cdot \boldsymbol{J} = 0$. The current density is defined simply by Ohm's law, $\boldsymbol{J} = -\sigma \nabla \phi$, where σ is the electrical conductivity and ϕ is the local potential (voltage). Each material phase has a different constant electrical conductivity. $LiCoO_2$ has an electrical conductivity that is strongly a function of its lithium concentration or state of charge.[30] However, this paper primarily studied fresh (not electrochemically cycled) $LiCoO_2$, so $\sigma_{LCO,fresh} = 10^{-6}$ S/cm. Additionally, the next sections will show measurements results during and after electrochemical cycling. The cycled lithium cobalt oxide has a higher electrical conductivity than in the uncycled (fresh) cathode, as discussed by Nishizawa et al.[30] Here, $\sigma_{LCO,cycled} = 10^{-3}$S/cm.[30] The simulations use the binder conductivity values from measurements on 40 wt% carbon black as a function of cycle number (Figure 11) as that is the closest to the cathode binder composition of 50 wt%. Compared to both $LiCoO_2$ and the binder, the solvent conductivity is extremely low; a value of $\sigma_{void} = 10^{-10}$S/cm is used.

The key electrical metric is the effective cathode electrical conductivity, $\bar{\sigma}$, which is calculated by applying a voltage across the domain in the z direction perpendicular to the current collector and then normalizing the mean current density by the applied mean electric field,

$$\bar{\sigma} = \frac{\frac{1}{\Omega}\int J_z d\Omega}{\phi_{appl}/L}. \quad [1]$$

Here, J_z is the z (in the direction of the applied voltage) component of the current density, Ω is the simulation volume, ϕ_{appl} is the applied voltage, and L is the length of the domain in the z dimension. This integral is calculated over the entire computational domain (Ω) consisting of solid, binder, and solvent (void) phases.

Because the binder uniformly and continuously coats the $LiCoO_2$ particles and is found between many of the particle contacts, it also had an overwhelming influence on the effective conductivity of the electrode by carrying an abundance of current. For composite binders with carbon black fractions of 20 wt% and above, the binder conductivity was measured to be at least an order of magnitude greater than the conductivity of cycled $LiCoO_2$ of 10^{-3}S/cm. Figure 14b shows that for those conductivity ratios, the current densities in the binder can be much greater than the $LiCoO_2$ particles. Simulations with 32 nm binder thickness and a starting binder:$LiCoO_2$ conductivity ratio of 1,000:1 predicted that if the binder conductivity decreases by 68%, then the effective conductivity of the cathode would decrease by 67%. Therefore, the effective cathode conductivity was predicted to be proportional to the binder electrical conductivity, in qualitative agreement with the observed experimental trends. A separate simulation where the binder:$LiCoO_2$ conductivity ratio was only 3.2:1, the binder phase carried nearly 25% of the total current of the entire electrode. When normalized by the volume of each phase, the *average* current density of the binder was almost twice that of the $LiCoO_2$.

Predicted electrical conductivities of an solvent-swollen composite cathode with 40 wt% carbon black in the PVDF are shown in Figure 15. Both fresh, fully-lithiated and electrochemically-cycled $LiCoO_2$ materials were considered in this figure through the different conductivities discussed previously. Three binder thicknesses (10 nm, 32 nm, and 100 nm) are shown.

In both the fresh and cycled cases, the effective conductivity of the cathode was larger when the binder coating was thicker. A thicker binder means more of the overall volume is binder and the binder's conductivity is significantly higher than the $LiCoO_2$ conductivity. The

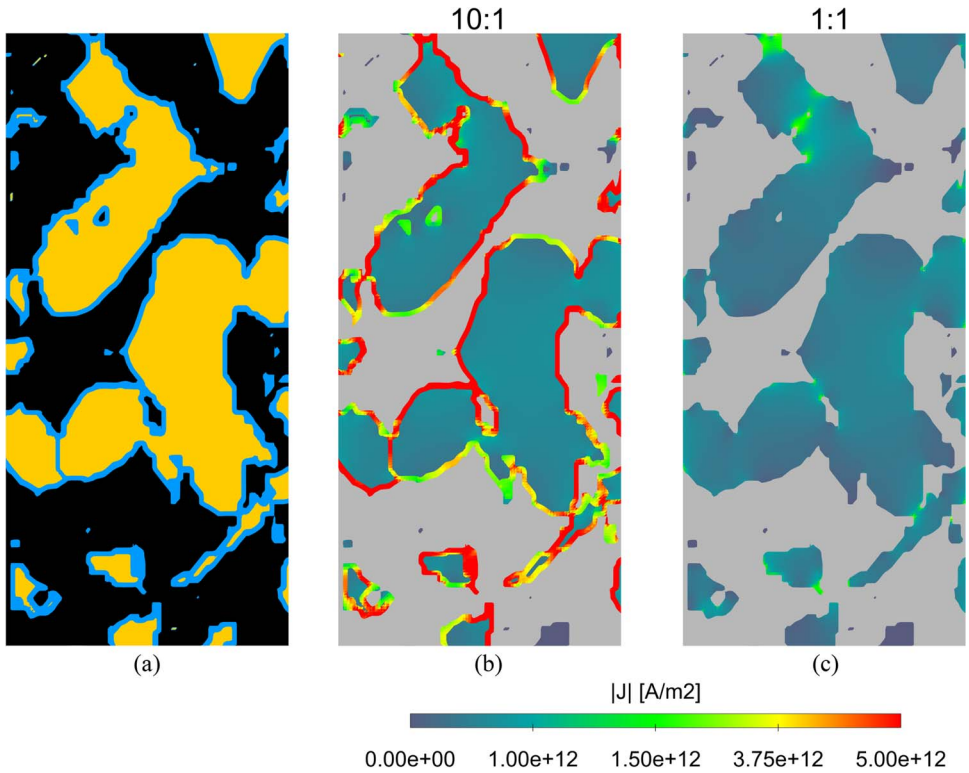

Figure 14. Simulated electrical conduction through a composite cathode generated by 3D reconstruction of experimental data. a) Binder is simulated as a uniform coating on the active material particles shown here for 100 nm binder thickness, b) Current density assuming a binder thickness of 100 nm. When the conductivity of the binder is 10x the conductivity of the active material, a vast majority of the current travels through the binder. This conductivity ratio is representative of an uncycled cathode. c) Even if the conductivities of the two phases are equal, the peak current densities are localized in the binder at the contact points between particles.

trends with respect to carbon black content and cycling were consistent with the cathode experimental data shown in Figure 13b.

Finally, Figure 15 shows that the cycled cathode was generally more conductive than the fresh cathode. The difference was more significant (in terms of percent change from the fresh cathode) when the binder was thinner, as the binder conductivity dominates over $LiCoO_2$ when there was more binder present.

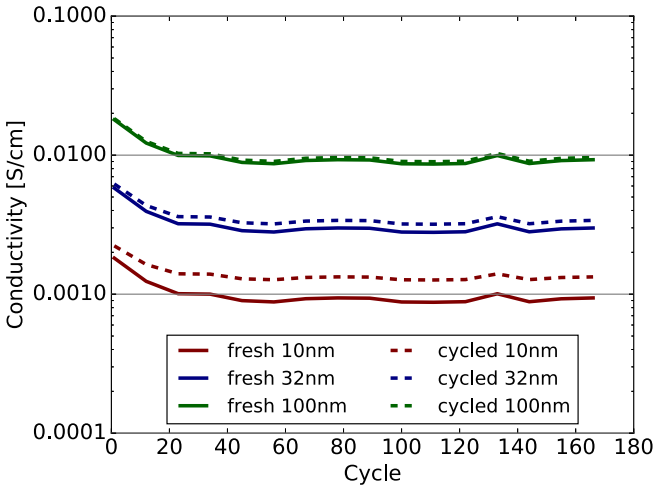

Figure 15. Simulated effective conductivity of a composite cathode using fully-lithiated (fresh) and electrochemically-cycled (cycled) $LiCoO_2$ conductivities and the swollen binder conductivities from Figure 13b. Three binder thicknesses are used, and binder conductivity as a function of cycle are taken from experiments on solvent swollen 40 wt% carbon black films.

Overall, the simulation predictions compared better than expected with the experimental measurements in Figure 13b especially given the small computational domain, idealized assumptions about binder morphology, and lack of a stress-conductivity coupling. It's worth noting that for the cycled simulations we degraded the conductivity of the entire binder coating, whereas in reality it is likely just the binder near the particle contacts that is subjected to the stresses that lead to changes in the conductivity. The simulations predict that for the experimental cathode composition, the effective conductivity of the cathode should decline proportionally to the decline of binder conductivity in agreement with the experimentally observed trends. The simulations do not allow for microstructure rearrangements, so binder degradation alone can cause the significant cathode conductivity degradation. Thus we conclude that the degradation in binder conductivity is the likely the mechanism of the observed decline in the cathode conductivity, suggesting that in the real cathodes there must be a significant amount of mechanically-stressed binder between the particles.

Electrochemical Cycling of $LiCoO_2$-Graphite Batteries

It has been hypothesized that mechanical stress induced by volume changes during lithiation and delithiation play a key role in battery degradation during cycling due to mechanically-driven degradation. The evolution of the internal resistance of a full coin-cell battery during electrochemical cycling was investigated and compared to the mechanically-driven degradation of the cathode. Coin cells were assembled using a similar $LiCoO_2$ cathode as previously tested, a graphite anode, and 1.2 M lithium hexafluorophosphate ($LiPF_6$) ethylene carbonate(EC):ethyl methyl carbonate (EMC) (3:7 w/w) electrolyte. Prior to testing, each cell was cycled for solid electrolyte interphase (SEI) formation at C/10 for five cycles between 3.0 and 4.2 V in constant current mode. Following this formation cycling, each cell was subjected to 50 cycles while using current interrupt

techniques to probe the cell resistance throughout each cycle. In a current interrupt test, periods of constant current and zero current (rest) are alternated between cutoff potentials of 3.0 V and 4.2 V. The rest period is four minutes while the duration of active current can vary depending on the applied rate. The various charging rates tested included 2C, C/2, C/5, and C/10. During the rest, the potential was measured and it was the initial potential change that was used to determine the ohmic resistance. Due to the experimental set-up and test limitations, the first potential measurement was typically ~20 ms after the interrupt. The ohmic resistance was calculated by dividing the initial potential change by the applied current. Although the resistance contains contributions from both the cathode and the anode, it was determined through half-cell testing that the $LiCoO_2$ electrode dominates the ohmic resistance compared to contributions from the graphite anode, likely due to the lower electronic conductivity of $LiCoO_2$ compared to graphite. Thus, the measured resistance of the full cell was expected to be representative of the cathode resistance.

The conductivity was calculated from the ohmic resistance, the electrode area and total electrode coating thickness (120 μm). The cell conductivity as a function of state of charge (SOC) is shown in Figure 16 for a charging rate of C/10. During this cycle, the ohmic resistance was on average 61% of the total resistance. For faster charging rates, the ohmic resistance constitutes a larger fraction of the total resistance (71% for C/2 and 80% for 2C rates). Note that the conductivity values for the full cell were almost an order of magnitude lower than the conductivity of the cathode measured previously. The differences were larger than we would expect if the electronic resistance was dominated by the cathode, potentially due to the additional sources of electronic resistance in a full cell or attributable to differences in measurement technique. The current interrupt method assumes that the cell resistance is real, but electrical impedance spectroscopy measurements on full batteries typically show that the resistance is complex which could make a direct comparison difficult. Because a battery is a complex load which shows capacitive and ohmic behavior, it is difficult to measure the internal resistance alone without other contributions from capacitive behavior. Considering the resistance was measured close to 20 ms after interrupt, there may have been additional contributions from non-electronic responses. Given the time constant equivalence of 50 Hz, contributions from the SEI were likely given its high-frequency behavior, however contributions from medium frequency elements such as charge-transfer should be insignificant here. Thus, we assume that SEI and solution resistance were not changing during cycling.

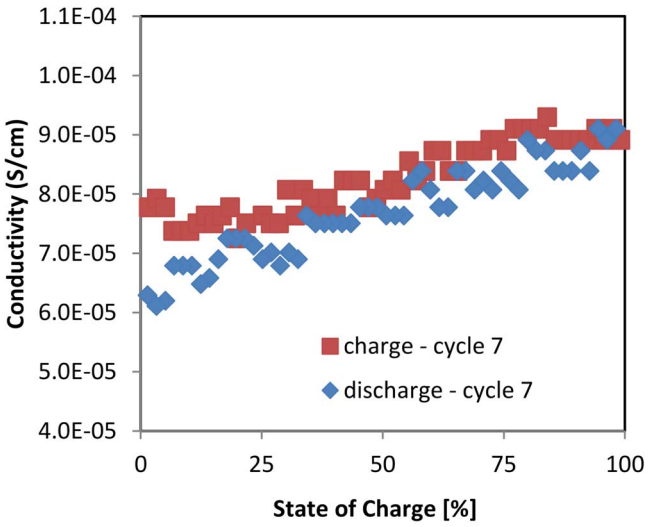

Figure 16. Measured cell conductivity as a function of state of charge measured by current interrupt testing at a charging rate of C/10. Results are shown for cycle #7 which includes the 5 formation cycles performed prior to current interrupt testing.

Figure 16 shows a modest dependence of the electrical conductivity on state of charge. There are several potential causes. As the cathode charged, the conductivity of the $LiCoO_2$ increased, possibly increasing the effective cathode conductivity similar to the predictions shown in Figure 15. Another mechanism suggested by Figure 4c was that as the cell charged and the anode and cathode swelled, the mechanical stress initially increased the conductivity of the binder. The dependence of the cell conductivity on state of charge decreased with cycling, a trend that was consistent with conductivity measurements of cycled binder as shown in Figure 6d. A change in ohmic resistance as a function of the state of charge has been previously reported in literature, although the cause was not ascertained.[33] Given the dependency, the average ohmic resistance between 0–10% SOC is reported, to better compare the resistance in the full cell to that reported for the uncycled cathode material.

The conductivity is reported as a function of cycle number for the various charging rates in Figure 17a. Both the total resistance and the ohmic resistance increased with cycling. The electronic resistance attributed to diffusion mechanisms also increased after cycling which could be evidence of restricted ionic conductivity due to consolidation of the electrodes caused by the cyclic mechanical stresses. The different cycle rates also affected the initial cell conductivity causing the various charging rates to be offset vertically from each other. There is not a direct analog to this behavior for the mechanical cycling testing. Thus for the purposes of comparison and to focus on the degradation patterns, we compare the cell conductivities normalized by the initial cell conductivity as shown in Figure 17b.

A now familiar trend was observed in the evolution of electronic conductivity during cycling. During 50 electrochemical cycles, the effective cell conductivity decreased by 12–26% compared to a decline of 31% in a cathode than had been mechanically cycled 56 times. The overpotential of the cell increased by 5–14 mV on charge and 5–35 mV on discharge. Figure 17b also compares the normalized conductivity of the electrochemically cycled cell to the mechanically cycled cathode. While cycle rates and applied stresses may differ between data sets (the dynamic stress in the coin cell is unknown), the comparison is still compelling. The mechanically- and electrochemically-cycled systems exhibited similar trends of electronic conductivity degradation, suggesting that mechanically-driven degradation of the binder may be a major contributor to increased ohmic resistance of the battery.

Conclusions

Lithium-ion batteries experience a complex mechanical environment. Not only are they packaged under a confinement stress, but as they are electrochemically cycled, the volume change of the battery active material causes cyclic mechanical stresses on the cell. Previously, the impact of that mechanical environment on the polymer composite binder had focused on the binder's mechanical role of holding the electrode together.[7] Here, we have demonstrated that the mechanical stresses within a lithium-ion battery due to volume changes that occur on lithiation can have a profound effect on the electrical properties of the composite polymer-carbon black binder. One might expect mechanical stress to improve battery performance and confinement stress is routinely applied to decrease battery internal resistance. Initially mechanical stress did increase the binder conductivity, presumably by increasing contact between the carbon black aggregates. Mechanical cycling also caused the binder films to become denser.

However, the cyclic mechanical stresses also caused large decreases in the electronic conductivity of the binder of 45–75% after 166 cycles. The degradation was consistent over various carbon black fractions, the presence or absence of absorbed solvent and the source of polyvinylidene fluoride polymer. The conductivity of the binder was dependent on the percolated carbon black network spanning the binder. At the macroscale, if cracks are formed within the binder, the conductive pathways could be blocked. At the microscale, the cyclic mechanical deformations could also either disrupt the percolated network or actually break apart the carbon black particles. Scanning

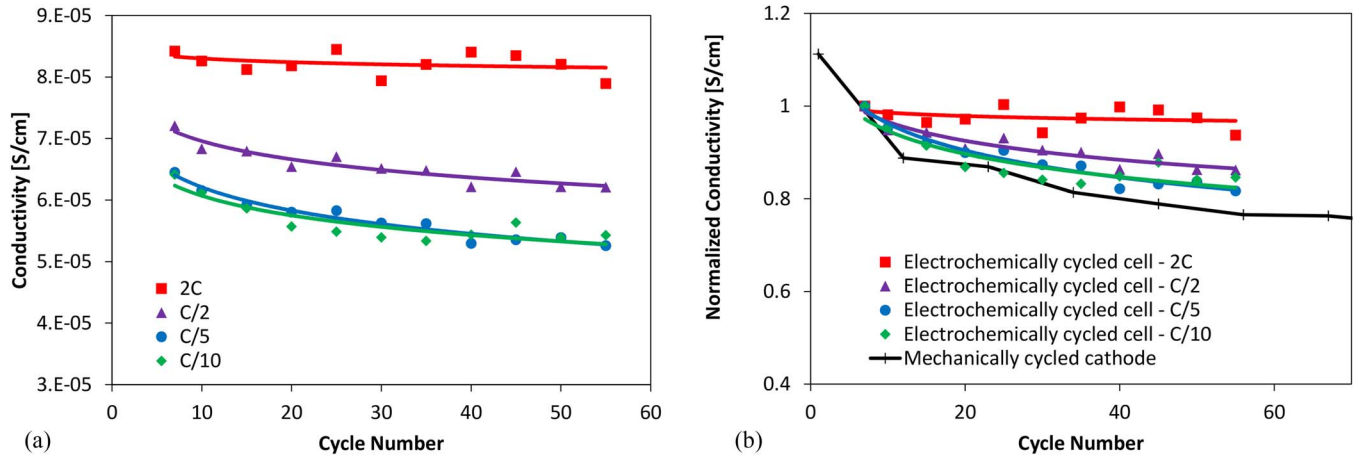

Figure 17. Measured reduction in the ohmic cell conductivity using current interrupt technique as a function of electrochemical cycling shows similar trends in the degradation of electrical conductivity due to cyclic mechanical stresses. Since the overall cell resistance is expected to be dominated by the cathode, the measured resistance is believed to be representative of cathode resistance. For C/10 rate, the average ohmic resistance comprises between 27–61% of the total resistance depending on cycle number. (a) Cell electrical conductivity as a function of cycle number; (b) Comparison of normalized electrical conductivity degradation for electrochemically cycled cells and mechanically cycled cathodes. For C/2, the average ohmic resistance is 54–71%.

electron images of uncycled and cycled binder films shown in Figures 1 and 9 show no obvious structural changes such as cracks, polymer delamination or other disruptions of the film morphology. At this time the physical mechanism for the conductivity degradation is not clear.

Since the binder is much more electrically conductive than the $LiCoO_2$ active material, binder conductivity degradation is expected to have the largest effect in the cathode. Experiments confirmed that the cathode electrical conductivity also degraded by 29-42% after 166 mechanical cycles. Simulations of effective electrical conductivity of cathodes have predicted that current density in the binder was generally much higher than in the active material due to the large differences in their conductivities. Simulations also showed that decreases in composite binder conductivity should translate directly into decreases in the cathode conductivity in agreement with experimental measurements of mechanical cycling degradation of cathodes. This evidence supports the hypothesis that the binder conductivity degradation is the likely cause for the conductivity degradation in the cathode.

Measurements of the internal ohmic resistance of a full $LiCoO_2$:graphite battery coin cell also showed conductivity degradation after electrochemical cycling. Based on halfcell measurements, we found that the major contributor to the cell resistance was the cathode. We assumed that after five formation cycles that changes in the SEI resistance and other sources of resistance could be neglected. In comparing the normalized conductivities for a full cell undergoing electrochemical cycling and a cathode undergoing purely mechanical cycling, we found that the degradation of the two systems were qualitatively consistent (12–26% for the full cell compared to 31% for the cathode). The combined evidence suggests that the mechanical stresses generated during electrochemical cycling are degrading the binder conductivity which in turn is decreasing the conductivity of the cathode and the battery cell as a whole. After just 50 cycles, the increase in overpotential attributed to the rise in ohmic resistance within the cell was 5–14 mV over a range of charging rates. If a constant current charging method is used, the increased overpotential will result in an effective capacity loss of up to 2%. Thus the changes in binder properties due to the mechanical stresses have a real and measurable impact on electrochemical performance of the battery through increased cell internal resistance.

The increased internal resistance can have important impacts for performance of rechargeable lithium-ion batteries. Developing rechargeable batteries that have stable and safe performance over thousands of cycles is a key research challenge. In particular, next generation high capacity anodes with large volume changes will only increase the mechanical stresses present in batteries. Understanding the impact of those mechanical stresses will be necessary to develop commercial batteries based on these materials. The strong coupling between the applied mechanical stresses and the electrical performance of the binder was a surprising result and shows that the mechanics and electrochemistry cannot be understood in isolation. Binder degradation leading to increased cell internal resistance will negatively impact high current applications and could lead to increased cell heating during operation, potentially affecting not only performance but safety of batteries. Since electronic and thermal conduction are generally linked, the thermal conduction could also be degraded which would compound the negative safety consequences for cycled batteries.

Acknowledgments

This work was funded as part of Sandia's Laboratory Directed Research and Development Program. The authors acknowledge the entire Lithium-Ion Battery Degradation LDRD team for many helpful discussions. Sandia National Laboratories is a multi-program laboratory managed and operated by Sandia Corporation, a wholly owned subsidiary of Lockheed Martin Corporation, for the U.S. Department of Energy's National Nuclear Security Administration under contract DE-AC04-94AL85000.

References

1. J.-M. Tarascon and M. Armand, *Nature*, **414**, 359 (2001).
2. W.-J. Zhang, *Journal of Power Sources*, **196**, 13 (2011).
3. T. Reddy, *Linden's Handbook of Batteries*, McGraw-Hill Education, 4 edition, ISBN 978-0071624213 (2010).
4. W. C. Chueh, F. El Gabaly, J. D. Sugar, N. C. Bartelt, A. H. McDaniel, K. R. Fenton, K. R. Zavadil, T. Tyliszczak, W. Lai, and K. F. McCarty, *Nano Letters*, **13**(3), 866 (2013).
5. D. Wang, X. Wu, Z. Wang, and L. Chen, *Journal of Power Sources*, **140**, 125 (2005).
6. Stephen J. Harris and P. Lu, *The Journal of Physical Chemistry C*, **117**(13), 6481 (2013).
7. D. Y. W. Yu, M. Zhao, and H. E. Hoster, *ChemElectrochem*, **2**, 1090 (2015).
8. W. H. Woodford, W. C. Carter, and Y.-M. Chiang, *Energy & Environmental Science*, **5**, 8014 (2012).
9. J. R. Dahn, R. Fong, and M. J. Spoon, *Physical Review B*, **42**(10), 6424 (1990).
10. G. G. Amatucci, J. M. Tarascon, and L. C. Klein, *Journal of The Electrochemical Society*, **143**(3), 1114 (1996).
11. R. S. Rubino, H. Gan, and E. S. Takeuchi, *Journal of The Electrochemical Society*, **148**(9), A1029 (2001).
12. Y. Qi and S. J. Harris, *Journal of The Electrochemical Society*, **157**(6), A741 (2010).
13. J. Cannarella and C. B. Arnold, *Journal of Power Sources*, **245**, 745 (2014).
14. C. Snyder, C. Apblett, A. Grillet, T. Beechem, and D. Duquette, *Journal of Electrochemistry Society*, **163**(6), A1036 (2016).

15. M. Qu, W. H. Woodford, J. M. Maloney, W. C. Carter, Y.-M. Chiang, and K. J. Van Vliet, *Advanced Energy Materials*, **2**, 940 (2012).
16. A. Linares and J. L. Acosta, *European Polymer Journal*, **33**(4), 467 (1997).
17. E. K. Rahani and V. B. Shenoy, *Journal of The Electrochemical Society*, **160**(8), A1153 (2013).
18. A. Awarke, S. Lauer, M. Wittler, and S. Pischinger, *Computational Material Science*, **50**, 871 (2011).
19. K. Takahashi, K. Higa, S. Mair, M. Chintapalli, N. Balsara, and V. Srinivasan, *Journal of the Electrochemical Society*, **163**(3), A385 (2016).
20. J. Brandrup, E. H. Immergut, and E. A. Grulke, editors. Polymer Handbook, Wiley Interscience, 4 edition, ISBN 0471-479365 (1999).
21. C. M. Costa, M. M. Silva, and L. Lanceros-Mendez, *RSC Advances*, **3**, 11404 (2013).
22. Z. Chen, L. Christensen, and J. R. Dahn, *Journal of Applied Polymer Science*, **90**, 1891 (2003).
23. M. Watanabe, M. Kanba, H. Matsuda, K. Tsunemi, K. Mizoguchi, E. Tsuchida, and I. Shinohara, *Die Makromolekulare Chemie, Rapid Communications*, **2**(12), 741 (1981).
24. G. Liu, H. Zheng, S. Kim, Y. Deng, A. M. Minor, X. Song, and V. S. Battaglia, *Journal of The Electrochemical Society*, **155**(12), A887 (2008).
25. G. Liu, H. Zheng, X. Song, and V. S. Battaglia, *Journal of The Electrochemical Society*, **159**(3), A214 (2012).
26. S. Babinec, H. Tang, A. Talik, S. Hughes, and G. Meyers, *Journal of Power Sources*, **174**(2), 508 (2007) 13th International Meeting on Lithium Batteries.
27. T. Hutzenlaub, S. Thiele, R. Zengerle, and C. Ziegler, *Electrochemical and Solid State Letters*, **15**(3), A33 (2012).
28. E. M. C. Jones, M. N. Silberstein, S. R. White, and N. R. Sottos, *Experimental Mechanics*, **54**, 971 (2014).
29. H. Mendoza, S. A. Roberts, V. E. Brunini, and A. M. Grillet. *Electrochimica Acta*, **190**, 1 (2016).
30. M. Nishizawa, S. Yamamura, T. Itoh, and I. Uchida, *Chemical Communications*, 1631 (1998).
31. P. K. Notz, S. R. Subia, M. M. Hopkins, H. K. Moffat, D. R. Noble, and T. O. Okusanya. Technical report SAND2016-4159, Sandia National Laboratories (2016).
32. S. A. Roberts, V. E. Brunini, K. N. Long, and A. M. Grillet, *Journal of The Electrochemical Society*, **161**(11), F3052 (2014).
33. D. Andre, M, Meiler, K. Steiner, C. Wimmer, T. Soczka-Guth, and D. Sauer, *Journal of Power Sources*, **196**, 5334 (2011).